Progress In Electromagnetics Research, Vol. 110, 329–352, 2010

AN ANALYTICAL SECOND-FDTD METHOD FOR EVALUATION OF ELECTRIC AND MAGNETIC FIELDS AT INTERMEDIATE DISTANCES FROM LIGHTNING CHANNEL

M. Izadi, M. Z. A. Ab Kadir, C. Gomes and W. F. Wan Ahmad

Centre of Excellence on Lightning Protection (CELP)
Faculty of Engineering, Universiti Putra Malaysia
43400 UPM, Serdang, Selangor, Malaysia

Abstract—Evaluation of electric and magnetic fields due to lightning discharge is important in determination of lightning induced voltage and power system protection especially to the distribution system. In this paper, by using dipole method, Maxwell equations and second order finite-difference time domain (later referred as a 2nd FDTD method) on two realistic return stroke currents, an algorithm for evaluation of electric fields is proposed, which is based on numerical methods in the time domain. Besides proving greater accuracy, it also allows the evaluation of electric and magnetic fields away from lightning channel. In addition, the comparison between simulation results and measured fields' wave shape showed that the proposed algorithm is in good agreement for evaluation of electric and magnetic fields due to lightning channel.

1. INTRODUCTION

Evaluation of lightning electric and magnetic fields in time domain is an important subject that can be applied for the estimation of induced over voltages due to indirect effects of lightning. Lightning energy may enter into power lines due to (a) resistive coupling (b) inductive coupling or (c) capacitive coupling. Resistive coupling is resulted by direct strokes in to the lines or via back-flashing caused by ground potential rise. Such direct coupling often gives rise to

Received 8 August 2010, Accepted 4 November 2010, Scheduled 25 November 2010
Corresponding author: Mohd Zainal Abidin Ab Kadir (mzainal@eng.upm.edu.my).

a current pulse. Inductive and capacitive coupling takes place via electromagnetic interactions, hence termed as induced effects. Such coupling gives rise to induced voltage pulses [1]. Induced effects are more prevalent than direct effects due to the higher number of lightning strikes per given time in the proximity of power lines than that into the lines. Various models have previously been proposed to evaluate electric and magnetic fields both in time domain and frequency domain. In this study, electric and magnetic fields are evaluated and validated by experimental results at intermediate distances (in the range from about 500 m to 10 km) from the lightning channel. Previous FDTD methods in the time domain are mostly applied for close distance from lightning channel [2].

Calculations of electromagnetic fields require the temporal variation of lightning current at the channel base and that along the channel. Therefore, a realistic model for prediction of current wave shape is expressed. Consequently, electric and magnetic fields are evaluated by using the dipole method and the proposed method, respectively.

In this study, the basic assumptions made are:

1. The lightning channel is normal to the ground surface.
2. The ground surface is flat.
3. The return stroke velocity along the lightning channel is constant.
4. No effects on the current or fields due to branches of the channel.
5. No effects of corona in the lightning channel on the current or fields.

2. RETURN STROKE CURRENT AT CHANNEL BASE

In most parts of the world, out of all the ground lightning, about 90% are negative flashes [3]. An analytical expression usually adopted to represent the channel-base current, whose specific wave shape and amplitude can be determined experimentally, is the one proposed by Heidler [1, 4, 5], and frequently referred to as the "Heidler function". Note that, other functions on return stroke current at channel base have been proposed, such Bruce and Golde function [1, 4] and Pierce function [4, 6]. In this study, the Diendorfer and Uman function [1] which is a modification of Heidler function was chosen. The simulated results are validated with field measurements done under triggered

lightning. This function is described by the following Equation (1).

$$i(0,t) = \left[\frac{i_{01}}{\eta_1} \frac{\left(\frac{t}{\Gamma_{11}}\right)^{n_1}}{1+\left(\frac{t}{\Gamma_{11}}\right)^{n_1}} \exp\left(\frac{-t}{\Gamma_{12}}\right) + \frac{i_{02}}{\eta_2} \frac{\left(\frac{t}{\Gamma_{21}}\right)^{n_2}}{1+\left(\frac{t}{\Gamma_{21}}\right)^{n_2}} \exp\left(\frac{-t}{\Gamma_{22}}\right) \right] \tag{1}$$

where $i_{01},\ i_{02}$ are the amplitudes of the channel base current, $\Gamma_{11},\ \Gamma_{12}$ are the front time constant, $\Gamma_{21},\ \Gamma_{22}$ are the decay-time constants, $n_1,\ n_2$ are the exponents $(2 \sim 10)$, $\eta_1,\ \eta_2$ are the amplitude correction factors.

Also, typical values for this return stroke current are given in Table 1 [7].

The current wave shapes, based on cases 1 to 4 in Table 1, are shown in Figure 1.

Table 1. Typical values for Diendorfer and Uman channel base current function [1, 7].

Case	i_{01} (kA)	i_{02} (kA)	Γ_{11} (μs)	Γ_{12} (μs)	Γ_{21} (μs)	Γ_{22} (μs)	n_1	n_2	V (m/s)	λ (km)
1	19.5	12	1	2	8	30	2	2	1×10^8	1.5
2	17	8	0.4	4	4	50	2	2	1×10^8	1.5
3	10.5	9	2	4.8	20	26	2	2	1.5×10^8	2
4	10.7	6.5	0.25	2.5	2	230	2	2	1.9×10^8	2

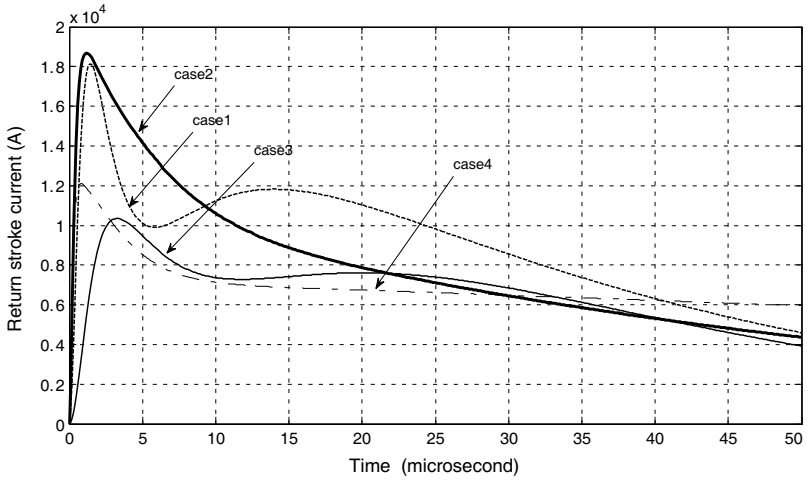

Figure 1. Return stroke current wave shape.

3. RETURN STROKE CURRENT WAVE SHAPE ALONG LIGHTNING CHANNEL

Several mathematical models have been developed to formulate the lightning current along the channel. Few such models are given below [1, 4, 8, 9]:

i) Bruce and Golde model or BG: The model assumes an infinite return stroke speed. There is no attenuation in the current pulse along the channel.

ii) Transmission Line model or TL: The model assumes a finite constant velocity for the return stroke with no attenuation of current pulse along the line.

iii) Traveling Current source model or TCS: The model assumes the speed of light for the return stroke. The return stroke tip acts as a upward travelling current source which transfers charge at each height to ground at infinite speed as the source reaches the given height. There is no attenuation of current pulse along the channel.

iv) Modified Transmission line with Exponential Decay model or MTLE: The model is similar to TL with the modification that the current pulse attenuates along the channel by a factor of $\exp(-z'/\lambda)$ where z' is the instantaneous height along lightning channel and λ is the decay constant which allows the current to reduce its amplitude with height. Note that, we use this model for the calculations in this study.

v) Modified Transmission Line with Linear Decay model or MTLL: model is similar to TL with the modification that the current pulse attenuates along the channel by a factor of $(1 - z'/H)$ where H is equal to cloud height.

So, the current amplitude correction factor in the BG, TL, TCS, MTLE, MTLL models are 1, 1, 1, $\exp(-z'/\lambda)$, $(1 - z'/H)$, respectively [1]. The experimental observations show that return stroke current reduces with height. Therefore, the model that assumes unit attenuation factor has an inherent drawback (BG, TCS and TL). Furthermore, it is unrealistic to assume an infinite speed for the flow of information such as in BG and TCS. Therefore, the MTLE and MTLL are the more realistic models compared with others. They also provide results which are in good agreement with experimental data.

The MTLE is given by the Equations (2) and (3) [1].

$$i\left(z', t\right) = i\left(0, t - z'/v\right) \exp\left(-z'/\lambda\right) \qquad z' \leq vt \tag{2}$$

$$i\left(z', t\right) = 0 \qquad z' > vt \tag{3}$$

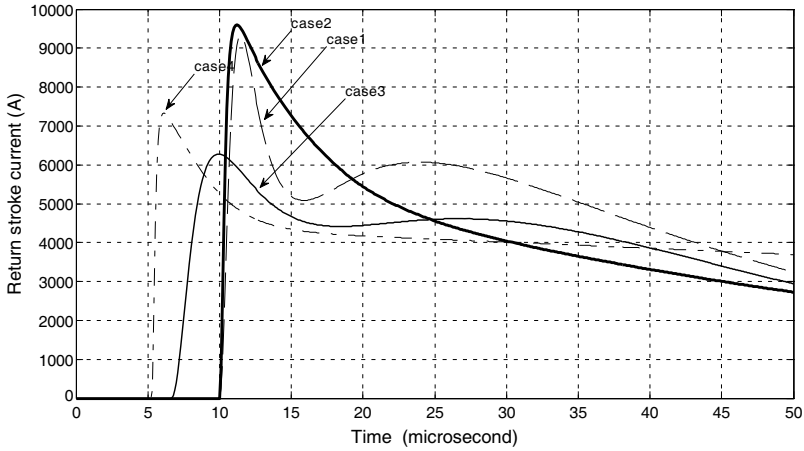

Figure 2. The temporal variation of the current at $z = 1000\,\mathrm{m}$ along the channel.

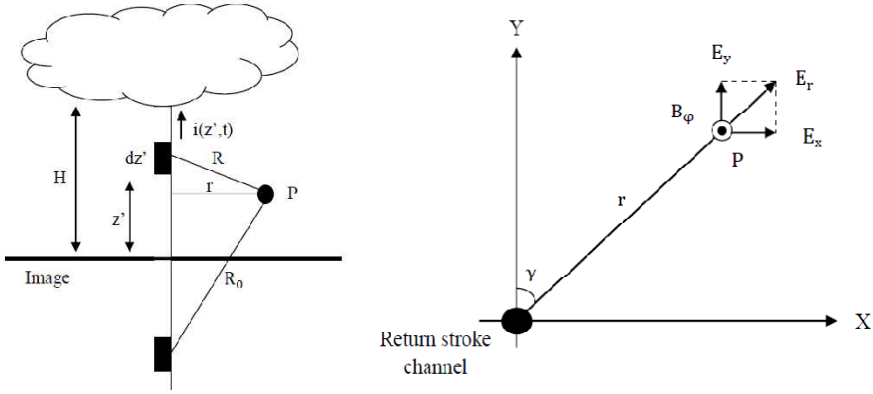

Figure 3. Geometrical parameters used in the calculations.

The temporal variation of the currents at $z = 1000\,\mathrm{m}$ along the channel as per MTLE is given in Figure 2. The calculations are based on the parameters given in Table 1. Note that, Return stroke current velocity is an effective parameter for evaluation of current wave shape along lightning channel; it is effective on initial time shift at TL, MTLE and MTLL models. On the other hand, the electromagnetic fields due to lightning channel are depended on return stroke velocity along lightning channel as shown in Equations (4) to (6). The common values for that are between $c/3$ to $2c/3$. Also, λ is more effective on the

attenuation of the height dependent factor in MTLE model because it determines rate of exponential factor for reducing of current amplitude along lightning channel.

4. ELECTRIC AND MAGNETIC FIELDS DUE TO LIGHTNING

According to antenna theory and dipole method, electric and magnetic fields at an observation point, due to lightning current are given by Equations (4) to (6) [1]. The equations are valid for infinite ground conductivity and flat horizontal ground surface. Figure 3 depicts geometric parameters pertinent to the model.

$$E_r(r,z,t) = \left(\frac{1}{4\pi\varepsilon_0}\right)\int_{-H'}^{H'}\left(\frac{3r\left(z-z'\right)}{R^5}\int_0^t i\left(z',\tau-\frac{R}{c}\right)d\tau + \frac{3r\left(z-z'\right)}{cR^4}i\left(Z',t-\frac{R}{c}\right) - \frac{r\left(z-z'\right)}{c^2R^3}\frac{\partial i\left(z',t-\frac{R}{c}\right)}{\partial t}\right)dz' \quad (4)$$

$$E_z(r,z,t) = \left(\frac{1}{4\pi\varepsilon_0}\right)\int_{-H'}^{H'}\left(\frac{2\left(z-z'\right)^2-r^2}{R^5}\int_0^t i\left(z',\tau-\frac{R}{c}\right)d\tau + \frac{2\left(z-z'\right)^2-r^2}{cR^4}i\left(z',t-\frac{R}{c}\right) - \frac{r^2}{c^2R^3}\frac{\partial i\left(z',t-\frac{R}{c}\right)}{\partial t}\right)dz' \quad (5)$$

$$B_\varphi(r,z,t) = \left(\frac{\mu_0}{4\pi}\right)\int_{-H'}^{H'}\left(\frac{r}{R^3}i\left(z',t-\frac{R}{c}\right) + \frac{r}{cR^2}\frac{\partial i\left(z',t-\frac{R}{c}\right)}{\partial t}\right)dz' \quad (6)$$

where

$$R = \sqrt{r^2+\left(z-z'\right)^2},$$
$$R_0 = \sqrt{r^2+\left(z+z'\right)^2},$$

$E_r(r,z,t)$ is the horizontal electric field at perfect ground conductivity, $E_z(r,z,t)$ is the vertical electric field at the perfect ground conductivity, $B_\varphi(r,z,t)$ is the magnetic flux density at the perfect ground conductivity, z is height of observation point, z' is the vertical space variable.

Analytical solving Equations (4) and (5) in time domain using a realistic current wave shape is complicated because Integration of the electrostatic part in the electrical field is complicated when the double-exponential Heidler expression is used [10]. Therefore, in most of the previous studies the equations are solved in frequency domain.

Equation (6) could easily be solved using Gauss-Lobatto quadrature method [11] which is a numerical technique. The relations between electric and magnetic fields in a closed area can be expressed by Maxwell's Equation (7) to (11) [12–14].

$$\frac{\partial \vec{B}}{\partial t} + \nabla \times \vec{E} = 0 \tag{7}$$

$$\nabla \times \vec{H} = \frac{\partial \vec{D}}{\partial t} + \vec{j} \tag{8}$$

$$\vec{B} = \mu_0 \vec{H} \tag{9}$$

$$\vec{D} = \varepsilon_0 \vec{E} \tag{10}$$

$$\vec{j} = \sigma \vec{E} \tag{11}$$

where: $\vec{j}$ is current density vector, $\vec{D}$ is electric flux density vector, $\vec{H}$ is magnetic field, $\vec{B}$ is magnetic flux density, σ is the medium conductivity, ε_0 is the permittivity of free space, μ_0 is the permeability of free space.

Magnetic flux density could be expressed by Equation (12) by using Equations (8) to (11) for an observation point on the ground level and assuming perfect ground conductivity [15–17].

$$\nabla \times \vec{B} = \mu_0 \left(j + \frac{\partial \vec{D}}{\partial t} \right) = \mu_0 \left(\sigma \vec{E} + \varepsilon_0 \frac{\partial \vec{E}}{\partial t} \right) \tag{12}$$

By solving curl function, Equation (12) is converted to Equations (13) to (15).

$$\frac{\partial E_y}{\partial t} = \frac{1}{\varepsilon_0 \mu_0} \left(\frac{\partial B_z}{\partial x} - \frac{\partial B_x}{\partial z} - \mu_0 \sigma E_y \right) \tag{13}$$

$$\frac{\partial E_x}{\partial t} = \frac{1}{\varepsilon_0 \mu_0} \left(\frac{\partial B_y}{\partial z} - \frac{\partial B_z}{\partial y} - \mu_0 \sigma E_x \right) \tag{14}$$

$$\frac{\partial E_z}{\partial t} = \frac{1}{\varepsilon_0 \mu_0} \left(\frac{\partial B_x}{\partial y} - \frac{\partial B_y}{\partial x} - \mu_0 \sigma E_z \right) \tag{15}$$

By referring to Figure 4, the relations between B_φ and B_x, B_y (for converting Cylindrical to Cartesian coordinates) could be presented in Equations (16) to (18). Also, the values of $\frac{\partial B_z}{\partial y}$, $\frac{\partial B_z}{\partial x}$ are equal to zero as lightning channel is along z-axis and it is plumb on x-y plane.

$$\sin\gamma = \frac{n\Delta x}{\sqrt{(m\Delta y)^2 + (n\Delta x)^2}} \tag{16}$$

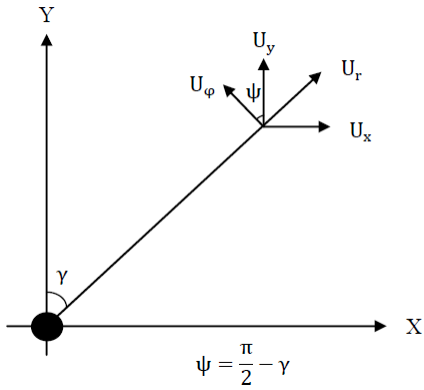

Figure 4. The chosen coordinate systems and unit vectors.

$$\cos\gamma = \frac{m\Delta y}{\sqrt{(m\Delta y)^2+(n\Delta x)^2}} \tag{17}$$

$$\vec{B} = -B_\varphi \sin\gamma U_y + B_\varphi \cos\gamma U_x \tag{18}$$

By applying 2nd FDTD method [18, 19], Equations (13) to (15) could be rewrite as per Equations (19) to (21), respectively. Note that, the observation point is at $(m\Delta y, n\Delta x, p\Delta z)$, the lightning channel is along z-axis and the processing time is equal to $k\Delta t$.

$$E_y^k(m,n,p) = \frac{-\varepsilon_0}{\sigma + \frac{3\varepsilon_0}{2\Delta t}} \left\{ \frac{E_y^{k-2}(m,n,p) - 4E_y^{k-1}(m,n,p)}{2\Delta t} + \frac{\cos\gamma_1}{\varepsilon_0\mu_0} \left(\frac{B_\varphi^k(m,n,p+1) - B_\varphi^k(m,n,p-1)}{2\Delta z} \right) \right\} \tag{19}$$

$$E_x^k(m,n,p) = \frac{-\varepsilon_0}{\sigma + \frac{3\varepsilon_0}{2\Delta t}} \left\{ \frac{E_x^{k-2}(m,n,p) - 4E_x^{k-1}(m,n,p)}{2\Delta t} - \frac{\sin\gamma_1}{\varepsilon_0\mu_0} \left(\frac{B_\varphi^k(m,n,p+1) - B_\varphi^k(m,n,p-1)}{2\Delta z} \right) \right\} \tag{20}$$

$$E_z^k(m,n,p) = \frac{-\varepsilon_0}{\sigma + \frac{3\varepsilon_0}{2\Delta t}} \left\{ \frac{E_z^{k-2}(m,n,p) - 4E_z^{k-1}(m,n,p)}{2\Delta t} - \frac{1}{\varepsilon_0\mu_0} \left(\frac{\cos\gamma_3 B_\varphi^k(m+1,n,p) - \cos\gamma_4 B_\varphi^k(m-1,n,p)}{2\Delta y} \right. \right.$$

$$-\frac{-\sin\gamma_5 B_\varphi^k(m,n+1,p)+\sin\gamma_6 B_\varphi^k(m,n-1,p)}{2\Delta x}\Bigg)\Bigg\} \quad (21)$$

where

$$\begin{aligned}
\cos\gamma_1 &= \frac{m\Delta y}{\sqrt{(m\Delta y)^2+(n\Delta x)^2}}\\
\sin\gamma_2 &= \frac{n\Delta x}{\sqrt{(m\Delta y)^2+(n\Delta x)^2}}\\
\cos\gamma_3 &= \frac{(m-1)\Delta y}{\sqrt{((m-1)\Delta y)^2+(n\Delta x)^2}}\\
\cos\gamma_4 &= \frac{(m+1)\Delta y}{\sqrt{((m+1)\Delta y)^2+(n\Delta x)^2}}\\
\sin\gamma_5 &= \frac{(n-1)\Delta x}{\sqrt{(m\Delta y)^2+((n-1)\Delta x)^2}}\\
\sin\gamma_6 &= \frac{(n+1)\Delta x}{\sqrt{(m\Delta y)^2+((n+1)\Delta x)^2}}
\end{aligned}$$

Magnetic flux densities in six points are evaluated using dipole method as expressed by Equation (6). Hence, by applying magnetic density values into Equations (19) to (21) all components of the electric field could be calculated. Computational stability requires the condition specified in Equation (22) [15]. Note that, $\Delta x = \Delta y = \Delta z < \lambda_e/10$ where λ_e is the wavelength.

$$\Delta t \le \frac{1}{c\times\sqrt{\frac{1}{(\Delta x)^2}+\frac{1}{(\Delta y)^2}+\frac{1}{(\Delta z)^2}}} \quad (22)$$

where c is equal to speed of light in free space.

In this method, the accuracy of results is increased by using 2nd FDTD method for solving Maxwell's equations. Figures 5 to 7 show magnetic flux density (B_φ), vertical electric field (E_z) and horizontal electric field (electric field along y-axis), respectively for an observation point of $x = 0$ m, $y = 9000$ m, $z = 10$ m of case 1 in Table 1. Note that, MTLE is employed in this case and ground conductivity is assumed to be perfect. Figures 8 and 9 show experimental measurements for magnetic flux density (B_φ) and vertical electric field (E_z) respectively at the observation point of $x = 0$ m, $y = 9000$ m, $z = 10$ m [7].

Table 2. Numerical comparison between magnetic flux density for measured and simulated values based on case 1 in Table 1.

Time (microsecond)	2	4	6	10	15	20	30
Magnetic flux density (measured values), Wb/m^2	1.28 $\times 10^{-7}$	0.9 $\times 10^{-7}$	0.62 $\times 10^{-7}$	0.6 $\times 10^{-7}$	0.45 $\times 10^{-7}$	0.42 $\times 10^{-7}$	0.42 $\times 10^{-7}$
Magnetic flux density (simulated values), Wb/m^2	1.32 $\times 10^{-7}$	0.85 $\times 10^{-7}$	0.58 $\times 10^{-7}$	0.61 $\times 10^{-7}$	0.58 $\times 10^{-7}$	0.45 $\times 10^{-7}$	0.3 $\times 10^{-7}$
Percentage difference, %	3	5	6	1	28	7	28

Table 3. Numerical comparison between vertical electric fields for measured and simulated values based on case 1 in Table 1.

Time (microsecond)	3	5	8	10	20	30	40
Vertical electric field (measured values), V/m	37.5	19	19.5	19	16	17	17.5
Vertical electric field (simulated values), V/m	38.8	18	18.5	18.8	16.5	14	13
Percentage difference, %	3	5	5	1	3	17	25

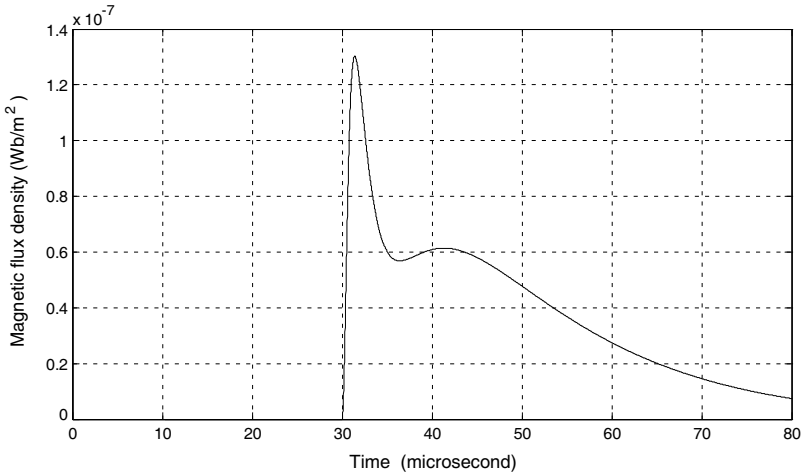

Figure 5. Simulation result for magnetic flux density (B_φ) at the observation point ($r = 9\,\text{km}$) calculated based on initial parameters of case 1 in Table 1.

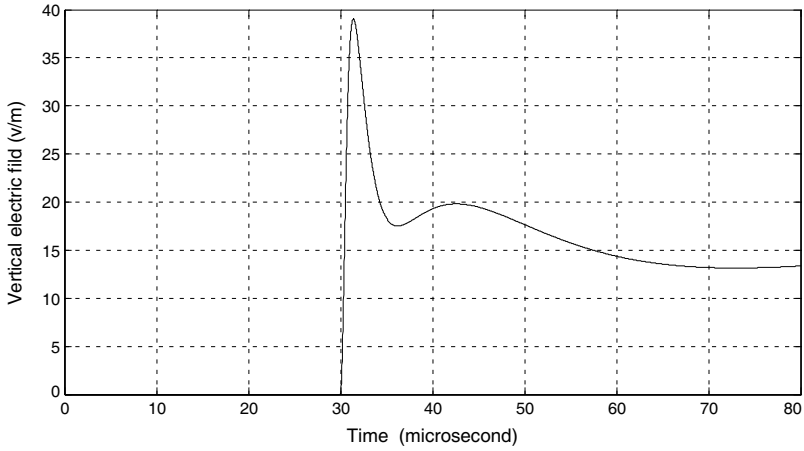

Figure 6. Simulation result for vertical electric field ($-E_z$) at the observation point ($r = 9\,\text{km}$) calculated by applying initial parameters that has been listed in case 1 of Table 1.

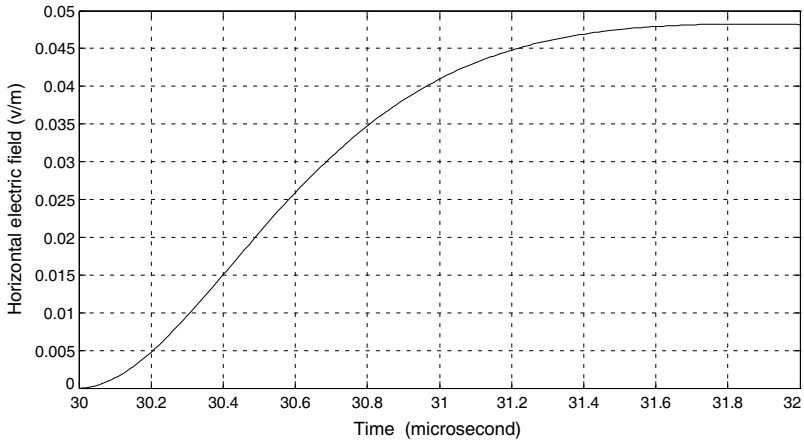

Figure 7. Simulation result for horizontal electric field (E_y — electric field along y-axis) at the observation point ($r = 9\,\text{km}$) calculated based on initial parameters of case 1 in Table 1.

On the other hand, the quantities comparison between simulation results and measured values for magnetic density and vertical electric field based on case 1 in Table 1 are listed in Tables 2 and 3, respectively. In simulation results, a delay time is observed in the field signatures. This time delay reflects the finite time required for the electric and

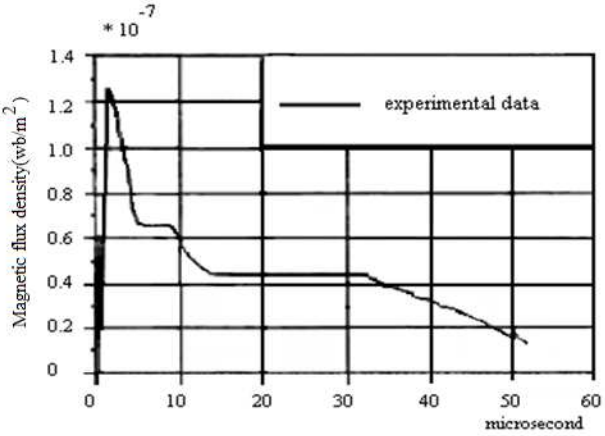

Figure 8. Experimental result for magnetic flux density (B_φ) at the observation point ($r = 9\,\text{km}$) calculated based on initial parameters of case 1 in Table 1 [7].

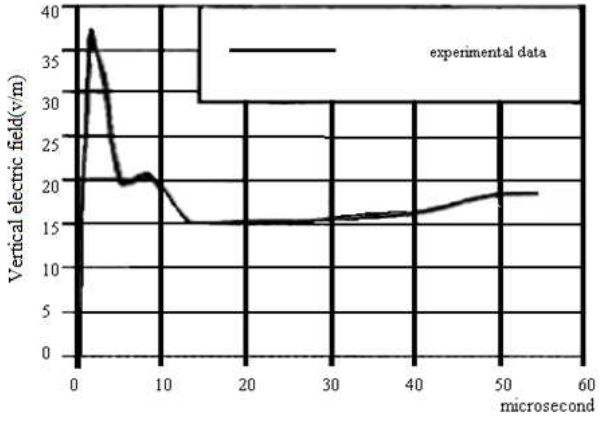

Figure 9. Experimental result for vertical electric field ($-E_z$) at the observation point ($r = 9\,\text{km}$) calculated based on initial parameters of case 1 in Table 1 [7].

magnetic fields to propagate from the channel to the location of the observation point (r/c). So for comparing measured and simulated values, it is necessary to subtract that delay time.

Figures 10 to 12 show magnetic flux density (B_φ), vertical electric field (E_z) and horizontal electric field (electric field along y-axis),

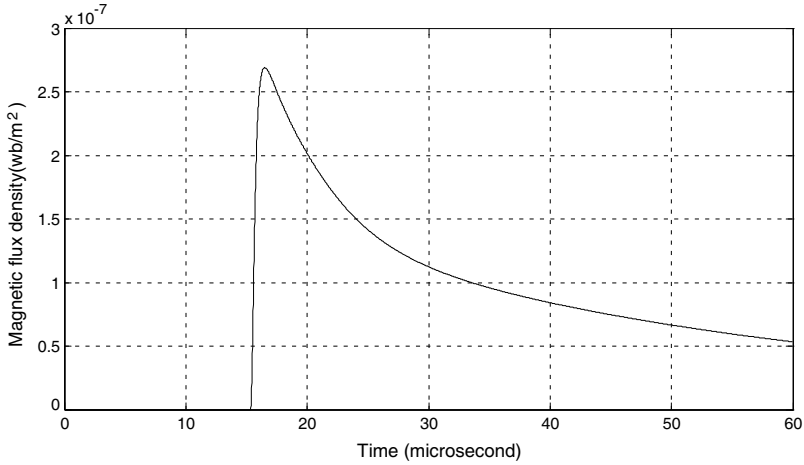

Figure 10. Simulation result for magnetic flux density (B_φ) at the observation point ($r = 4.6\,\text{km}$) calculated based on initial parameters of case 2 in Table 1.

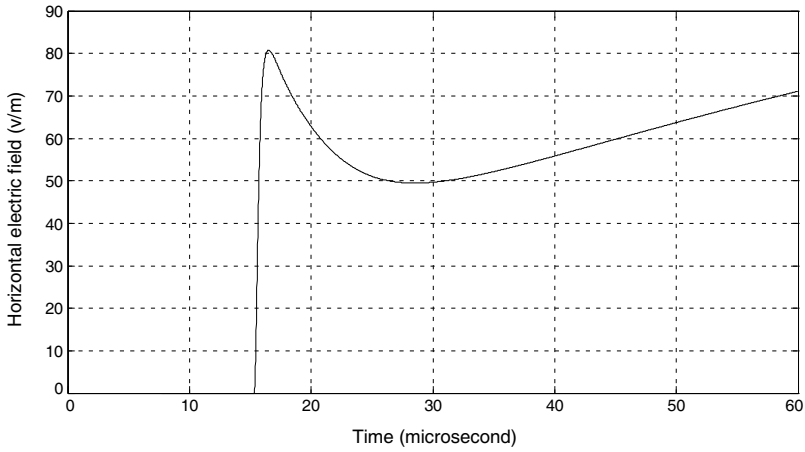

Figure 11. Simulation result for vertical electric field ($-E_z$) at the observation point ($r = 4.6\,\text{km}$) calculated based on initial parameters of case 2 in Table 1.

respectively for an observation point at $x = 0\,\text{m}$, $y = 4600\,\text{m}$, $z = 10\,\text{m}$ for case 2 of Table 1 parameters. Figures 13 and 14 show experimental results for magnetic flux density (B_φ) and vertical electric field (E_z), respectively at observation point of $x = 0\,\text{m}$, $y = 4600\,\text{m}$, $z = 10\,\text{m}$ [7]. Note that, MTLE is applied in this case and ground conductivity is assumed to be perfect.

Table 4. Numerical comparison between magnetic flux density for measured and simulated values based on case 2 of Table 1.

Time (microsecond)	2	5	8	10	15	25	35
Magnetic flux density (measured values), Wb/m^2	2.75×10^{-7}	2×10^{-7}	1.7×10^{-7}	1.5×10^{-7}	1.3×10^{-7}	0.9×10^{-7}	0.7×10^{-7}
Magnetic flux density (simulated values), Wb/m^2	2.7×10^{-7}	1.94×10^{-7}	1.6×10^{-7}	1.4×10^{-7}	1.25×10^{-7}	0.8×10^{-7}	0.75×10^{-7}
Percentage difference, %	2	3	6	6	4	11	7

Table 5. Numerical comparison between vertical electric fields for measured and simulated values based on case 2 of Table 1.

Time (microsecond)	3	10	15	20	25	35
Vertical electric field (measured values), V/m	81	53	53	58	58	75
Vertical electric field (simulated values), V/m	80	51	50	54	62	63
Percentage difference, %	1	4	5	7	6	16

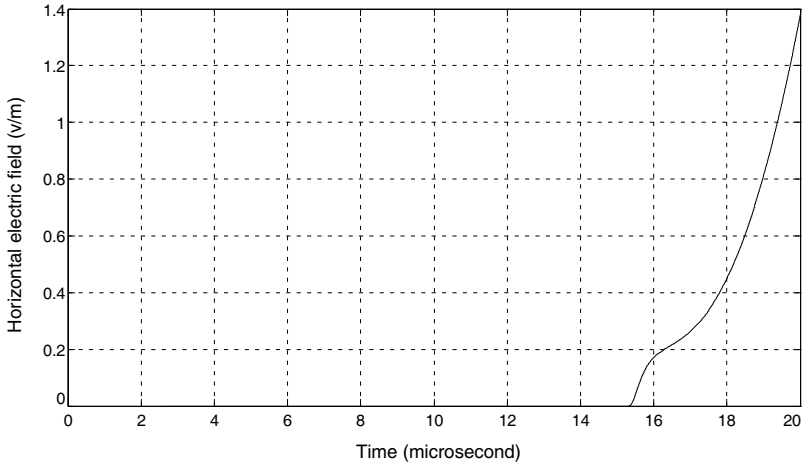

Figure 12. Simulation result for horizontal electric field (E_y — electric field along y-axis) at the observation point ($r = 4.6\,\text{km}$) calculated based on initial parameters of case 2 in Table 1.

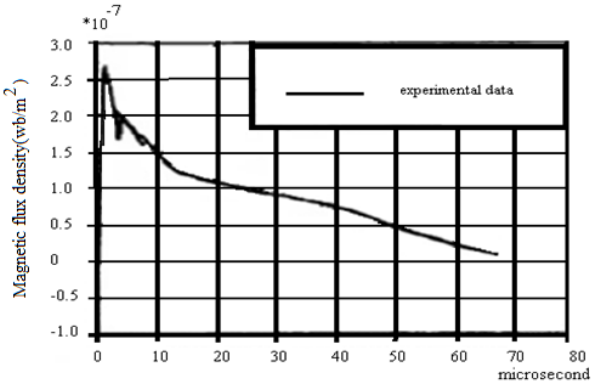

Figure 13. Experimental result for magnetic flux density (B_φ) at the observation point ($r = 4.6\,\text{km}$) calculated based on initial parameters of case 2 in Table 1 [7].

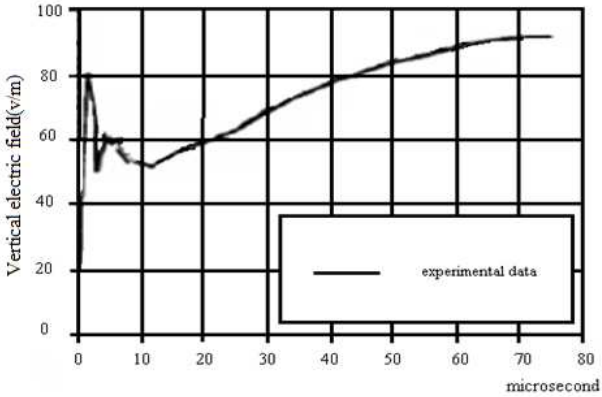

Figure 14. Experimental result for vertical electric field ($-E_z$) at the observation point ($r = 4.6\,\text{km}$) calculated based on initial parameters of case 2 in Table 1 [7].

Whilst Tables 4 and 5 show the quantities comparison between simulation results and measured values in the case 2 of Table 1 for magnetic flux density and vertical electric field, respectively.

Figures 15, 16, 19 and 20 show B_φ, E_z, respectively for two observation points at $x = 0\,\text{m}$, $y = 2000\,\text{m}$, $z = 10\,\text{m}$ (case 3 in Table 1) and $x = 0\,\text{m}$, $y = 50\,\text{m}$, $z = 10\,\text{m}$ (case 4 in Table 1) obtained using MLTE model and with the assumption of perfect ground conductivity. Also, Figures 17 and 18 demonstrate experimental results related to

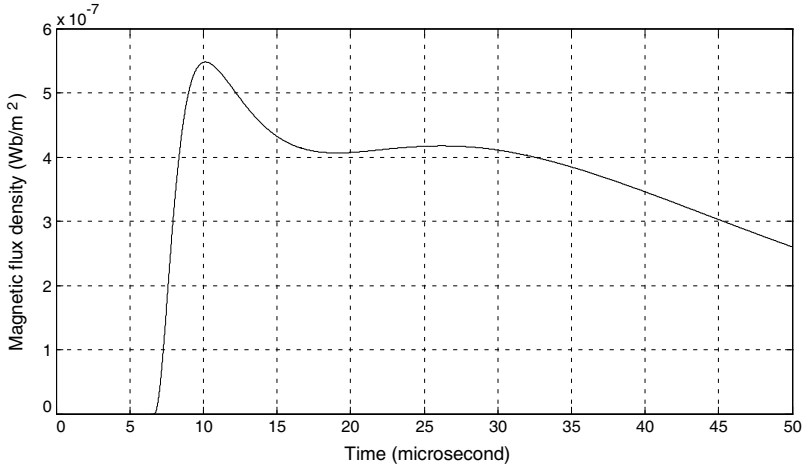

Figure 15. Simulation result for magnetic flux density (B_φ) at the observation point ($r = 2\,\text{km}$) calculated based on initial parameters of case 3 in Table 1.

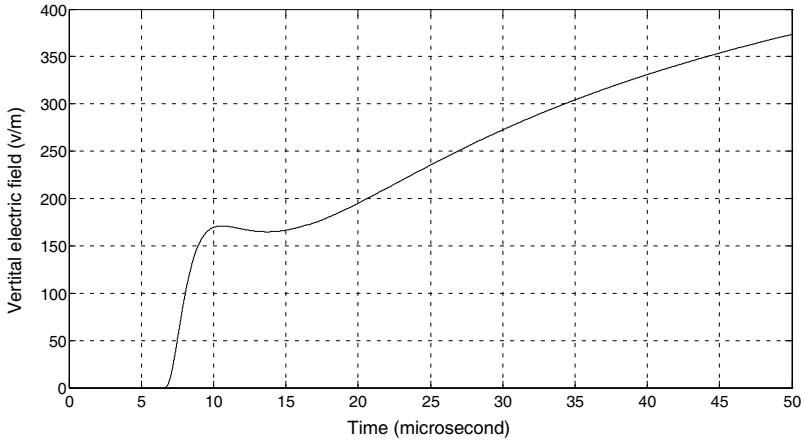

Figure 16. Simulation result for vertical electric field ($-E_z$) at the observation point ($r = 2\,\text{km}$) calculated based on initial parameters of case 3 in Table 1.

Figures 15 and 16, respectively. Whilst Figures 20 and 21 illustrate B_φ and E_z for validation of proposed method, using dipole method associated to Figures 19 and 20, respectively.

In addition, Tables 6 and 7 illustrate the quantities comparison between simulation results and measured values for case 3 of Table 1

Table 6. Numerical comparison between magnetic flux density for measured and simulated values based on case 3 of Table 1.

Time (microsecond)	3	10	15	20	30	40
Magnetic flux density (measured values), Wb/m^2	5×10^{-7}	3.3×10^{-7}	3.5×10^{-7}	3×10^{-7}	2.8×10^{-7}	2.6×10^{-7}
Magnetic flux density (simulated values), Wb/m^2	5.5×10^{-7}	4.1×10^{-7}	4.15×10^{-7}	4.1×10^{-7}	3.4×10^{-7}	2.8×10^{-7}
Percentage difference, %	10	24	18	24	21	7

Table 7. Numerical comparison between vertical electric fields for measured and simulated values based on case 3 of Table 1.

Time (microsecond)	3	10	15	20	30	40
Vertical electric field (measured values), V/m	180	175	235	260	310	360
Vertical electric field (simulated values), V/m	170	165	210	265	320	370
Percentage difference, %	5	5	10	2	3	3

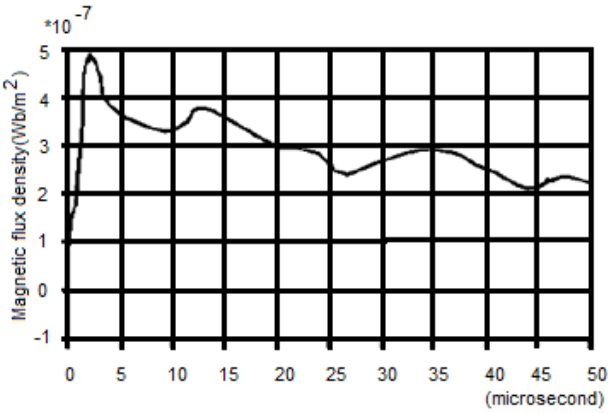

Figure 17. Experimental result for Magnetic flux (B_φ) at the observation point ($r = 2\,\text{km}$) calculated based on initial parameters of case 3 in Table 1 [7].

for magnetic flux density and vertical electric field, respectively.

Consideration on simulation results and measured values for case 3 of Table 1 exhibit that the magnetic flux density has a good agreement

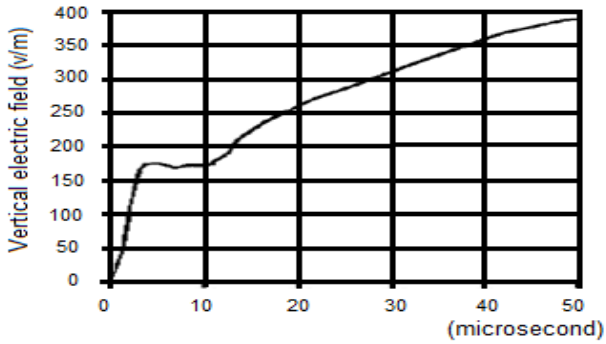

Figure 18. Experimental result for vertical electric field ($-E_z$) at the observation point ($r = 2\,\text{km}$) calculated based on initial parameters of case 3 in Table 1 [7].

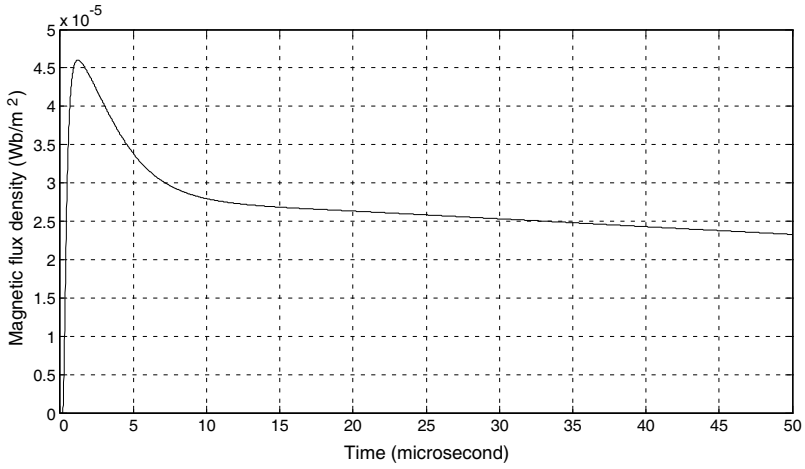

Figure 19. Simulation result for magnetic flux density (B_φ) at the observation point ($r = 50\,\text{m}$) calculated based on initial parameters of case 4 in Table 1.

until it reaches at the peak of field. With the time increases, percentage difference is increased. On the other hand, simulation results for vertical electric field have also demonstrated reasonably good results compared to the measured values in various time. Increment in the percentage difference could be due to the return stroke current model employed (MTLE), numerical method used in proposed method and percentage error during the experimental measurements.

Tables 8 and 9 demonstrate the quantities comparison between

Table 8. Numerical comparison between magnetic flux density for measured and simulated values based on case 4 of Table 1.

Time (microsecond)	2	10	20	30	40	50
Magnetic flux density (simulated values), $\mathrm{Wb/m^2}$	4.7 $\times 10^{-7}$	2.83 $\times 10^{-7}$	2.63 $\times 10^{-7}$	2.52 $\times 10^{-7}$	2.4 $\times 10^{-7}$	2.35 $\times 10^{-7}$
Magnetic flux density (from reference [1]), $\mathrm{Wb/m^2}$	4.6 $\times 10^{-7}$	2.8 $\times 10^{-7}$	2.6 $\times 10^{-7}$	2.5 $\times 10^{-7}$	2.4 $\times 10^{-7}$	2.3 $\times 10^{-7}$
Percentage difference, %	2	1	1	1	0	2

Table 9. Numerical comparison between vertical electric fields for measured and simulated values based on case 4 of Table 1.

Time (microsecond)	2	10	20	30	40	50
Vertical electric field (simulated values), V/m	22	26	37	47	58	67
Vertical electric field (from reference [1]), V/m	21	25	36	46	56	64
Percentage difference, %	4	4	2	2	3	4

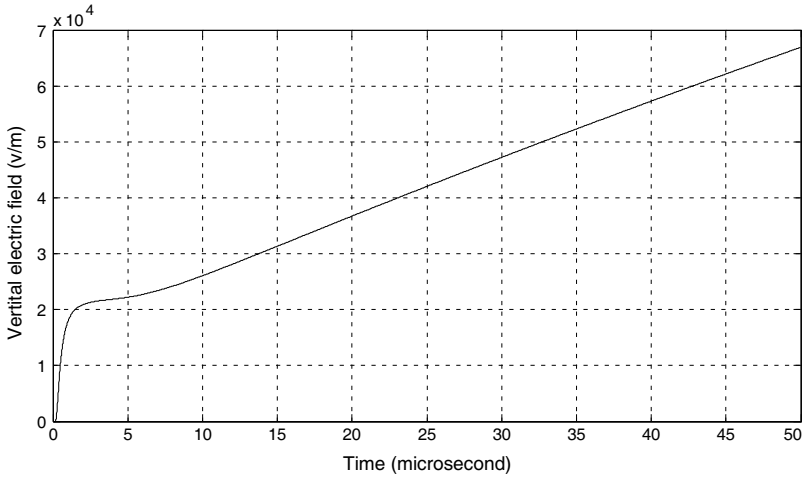

Figure 20. Simulation result for vertical electric field ($-E_z$) at the observation point ($r = 50\,\mathrm{m}$) calculated based on initial parameters of case 4 in Table 1.

simulation results and other calculation method (dipole method) values for validation of proposed method based on case 3 in Table 1 for magnetic flux density and vertical electric field, respectively.

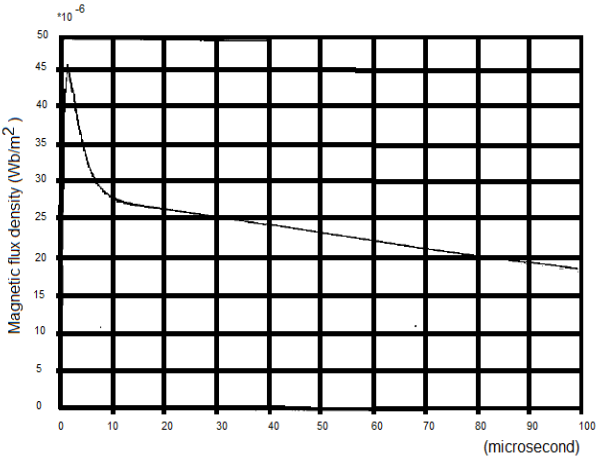

Figure 21. Magnetic flux (B_φ) based on dipole method at the observation point ($r = 50\,\mathrm{m}$) calculated based on initial parameters of case 4 in Table 1 [1].

Proposed method is validated with other simulation method as shown in Figures 19 to 22. Since both the simulation and experimental results are in good agreement as illustrated in Figures 5 to 18, it is reasonable to say that the developed algorithm is proved to be useful for the evaluation of electric and magnetic field due to lightning channel. On the other hand, the illustrated results also showed that this model can provide reasonably good results for evaluation of the fields with close and intermediate distances from the lightning channel. As the method described above carry out all the calculations in time-domain, the algorithm can be applied in many other areas such as the calculation or evaluation of voltages induced in power lines and determination of electric and magnetic fields, current and voltage induced to human body due to indirect strike.

This method has three advantages compared to the previous numerical methods that are used to calculate the electric and magnetic fields due to lightning channel using FDTD in time domain. They are listed as follows:

1. The proposed method is based on the combination of dipole method and Maxwell equations. Therefore, the required points for evaluation of fields at observation point are lesser compared to FDTD method. In the FDTD method, the plane is girded by four boundary conditions, i.e., lightning channel, ground surface

and two other boundary conditions before further divided into more small areas so for evaluation of electric and magnetic fields at observation point. This is explained in Figure 23 [2].
In this case, the information should be transferred layer by layer from boundary conditions to the observations point. Therefore, by increasing distance from lightning channel or observation point height, the number of layers will increase and so with the required memory. Note that each layer produces an error when transferring

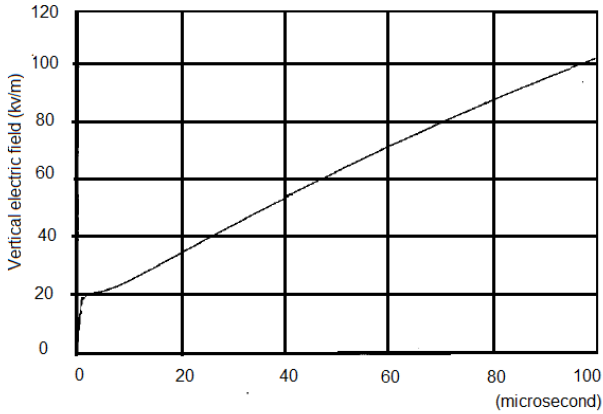

Figure 22. Vertical electric field $(-E_z)$ based on dipole method at the observation point $(r = 50\,\text{m})$ calculated based on initial parameters of case 4 in Table 1 [1].

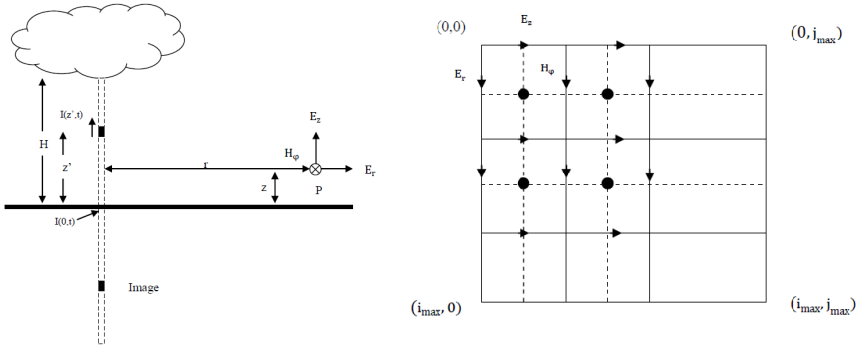

Figure 23. Geometry of FDTD method for evaluation of electric and magnetic fields at observation point [2].

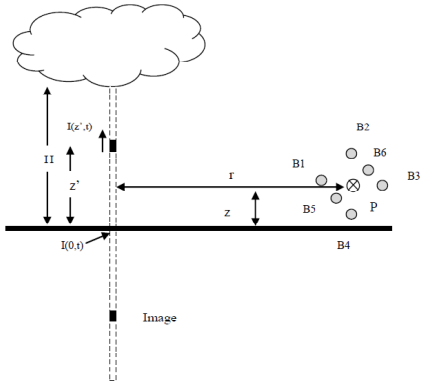

Figure 24. Geometry of proposed method for evaluation of electric fields at observation point.

data due to the fact that they are based on equations that solved by FDTD method, which has some errors. Whilst in the proposed method, dipole technique is used and estimation of magnetic flux density for six points around observation point, the electric fields are calculated as shown in Figure 24.

2. The FDTD method has only been validated for close distances from lightning channel [2] but this proposed method covered the intermediate distances from lightning channel. This is due to the magnetic flux density which is estimated based on dipole method and the fact that this method is validated for intermediate distances from lightning channel. In addition, electric fields are calculated using Maxwell's equations and therefore the proposed method provides good results for away distances calculation from lightning channel.
3. For solving Maxwell's equations, 2nd FDTD method is used (as shown in Figure 24) and hence gives better accuracy of results with the reduction in error percentage.

Another advantage is that this algorithm can also be integrated with the Agrawal coupling model due to the use of Cartesian coordinates in its electric fields calculation.

5. CONCLUSION

Indirect effect of lightning on the power lines is a major problem in the protection and insulation coordination cases for both power and communication equipments. The return stroke current produces

electromagnetic fields which then couple with power lines and induces an overvoltage which can cause damage to those equipments. Various models have been considered for an evaluation of electric and magnetic fields due to lightning channel but by applying realistic wave shape for return stroke current at channel base, those models became more complicated. Therefore, using Fourier transform and numerical methods in time domain, it provides a good solution for using realistic current wave shape. Different numerical methods based on Maxwell's equations are proposed for evaluation of electric and magnetic field due to lightning. This paper showed that by combining the dipole method and Maxwell's equations, (and then applies the numerical techniques on dipole method for estimation of magnetic flux density), the electric fields can be estimated by Maxwell's equations and 2nd FDTD method in time domain. With the advantages of the proposed method as compared to ordinary FDTD method, one can clearly notice that it provides faster solution in time domain with a very good agreement when compared with the measured results.

REFERENCES

1. Nucci, C. A., "Lightning-induced voltages on overhead power lines. Part I: Return stroke current models with specified channel-base current for the evaluation of the return stroke electromagnetic fields," *Electra*, Vol. 161, 75–102, 1995.
2. Yang, C. and B. Zhou, "Calculation methods of electromagnetic fields very close to lightning," *IEEE Transactions on Electromagnetic Compatibility*, Vol. 46, 133–141, 2004.
3. Uman, M., *The Lightning Discharge*, Dover Pub., 2001.
4. Rakov, V. and M. Uman, "Review and evaluation of lightning return stroke models including some aspects of their application," *IEEE Transactions on Electromagnetic Compatibility*, Vol. 40, 403–426, 1998.
5. Heidler, F., "Analytische blitzstromfunktion zur LEMP-berechnung," *18th ICLP*, 63–66, Munich, Germany, 1985.
6. Pierce, E. T., "Triggered lightning and some unsuspected lightning hazards (Lightning triggered by man and lightning hazards)," *ONR Naval Res. Rev.*, Vol. 25, 1972.
7. M'ziou, L., A. Mokhnache, A. Boubakeur, and R. Kattan, "Validation of the Simpson-finite-difference time domain method for evaluating the electromagnetic field in the vicinity of the lightning channel initiated at ground level," *IET*, Vol. 3, 279–285, 2009.

8. Djalel, H. A. D. and C. Benachiba, "Coupling phenomenon between the lightning and high voltage networks," *Proceedings of Word Academy of Science, Engineering and Technology (WASET)*, Vol. 21, 95–101, 2007.
9. Heidler, F., "Travelling current source model for LEMP calculation," *6th Symposium and Technical Exhibition on Electromagnetic Compability*, 157–162, Zurich, 1985.
10. Feizhou, Z. and L. Shanghe, "A new function to represent the lightning return stroke currents," *IEEE Transactions on Electromagnetic Compability*, Vol. 44, 2002.
11. Eslahchi, M. R., M. Masjed-Jamei, and E. Babolian, "On numerical improvement of Gauss-Lobatto quadrature rules," *Applied Mathematics and Computation*, Vol. 164, 707–717, 2005.
12. Zhou, X., "On independence completeness of Maxwell's equations and uniqueness theorems in electromagnetics," *Progress In Electromagnetic Research*, Vol. 64, 117–134, 2006.
13. Chen, J. and Q. H. Liu, "A non-spurious vector spectral element method for Maxwell's equations," *Progress In Electromagnetics Research*, Vol. 96, 205–215, 2009.
14. Zhang, Y.-Q. and D.-B. Ge, "A unified FDTD approach for electromagnetic analysis of dispersive objects," *Progress In Electromagnetics Research*, Vol. 96, 155–172, 2009.
15. Sadiku, M. N. O., *Numerical Techniques in Electromagnetics*, 2nd Edition, Ch. 3, CRC Press, 2001.
16. Young, J. L., R. O. Nelson, and D. V. Gaitonde, "A detailed examination of the finite-volume, time-domain method for Maxwell's equations," *Progress In Electromagnetic Research*, Vol. 28, 231–255, 2000.
17. Sartori, C. and J. Cardoso, "An analytical-FDTD method for near LEMP calculation," *IEEE Transactions on Magnetics*, Vol. 36, 1631–1634, 2000.
18. Silva-Macêdo, J. A., M. A. Romero, and B.-H. V. Borges, "An extended FDTD method for the analysis of electromagnetic field rotators and cloaking devices," *Progress In Electromagnetics Research*, Vol. 87, 183–196, 2008.
19. Jiang, Y.-N., D.-B. Ge, and S.-J. Ding, "Analysis of TF-SF boundary for 2D-FDTD with plane P-wave propagation in layered dispersive and lossy media," *Progress In Electromagnetics Research*, Vol. 83, 157–172, 2008.